JEMAT, 2025, Vol 13, No 1, 66-76
https://doi.org/10.54987/9qprpv83

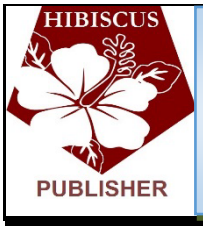

JOURNAL OF ENVIRONMENTAL MICROBIOLOGY AND TOXICOLOGY
Website: http://journal.hibiscuspublisher.com/index.php/JEMAT/index

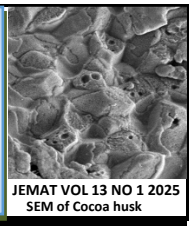

Fungal Biomass Immobilized on Polyacrylamide for the Adsorption of Chromium Ions

Ismail Haruna[1,2], Mohd Ezuan Khayat[1], Nur Adeela Yasid[1], Ain Aqilah Basirun[1] and M.Y. Shukor[1]*

[1]Department of Biochemistry, Faculty of Biotechnology and Biomolecular Sciences, Universiti Putra Malaysia, 43400 UPM Serdang, Selangor, Malaysia.
[2]Department of Microbiology, Faculty of Sciences, Sa'adu Zungur University, PMB 065 Itas/Gadau, Bauchi, Nigeria.

*Corresponding author:
Mohd Yunus Shukor,
Department of Biochemistry,
Faculty of Biotechnology and Biomolecular Sciences,
Universiti Putra Malaysia,
43400 UPM Serdang,
Selangor,
Malaysia.
Email: mohdyunus@upm.edu.my

History

Received: 11th March 2025
Received in revised form: 21st May 2025
Accepted: 30th June 2025

Keywords

Cr(VI)
Fungal biomass
Polyacrylamide immobilization
Brouers–Sotolongo isotherm
MOORA ranking

Abstract

Chromium pollution is a serious environmental problem because hexavalent chromium (Cr(VI)) is highly soluble, mobile, and toxic in aquatic systems. Using low-cost biosorbents in adsorption-based remediation proffers a prosperous treatment strategy, especially when stable polymeric matrices such as polyacrylamide are used to immobilize fungal biomass to improve operational stability, handling, and recovery. MOORA-based model ranking and nonlinear isotherm modelling are employed in this study to evaluate the equilibrium adsorption of Cr(VI) onto polyacrylamide-immobilized fungal biomass. Cr(VI) adsorption capacity continues to increase with an increase in equilibrium concentration and then follows an apparent plateau at higher C_e values, suggesting gradual binding of chromium species at available binding sites and an approach toward saturation. According to the MOORA ranking, the best-performing model was the Brouers–Sotolongo model. The maximum adsorption capacity of the Brouers-Sotolongo model was 76.33 mg/g (95% confidence interval from 51.29 to 101.37 mg/g) while the Langmuir model estimated the maximum adsorption at 68.05 mg/g (95% confidence interval from 61.89 to 75.11 mg/g). The potential of polyacrylamide-immobilized fungal biomass for Cr(VI) adsorption is demonstrated.

INTRODUCTION

Chemical speciation of chromium has a significant impact on the element's environmental risk. Because it is easily transported, hexavalent chromium is frequently found in a variety of environmental settings in aqueous systems as chromate or dichromate oxyanions. On the other hand, the less soluble trivalent chromium may bind firmly to the surfaces of minerals and organic materials or precipitate. This distinction causes a lot of remediation techniques to either try direct removal of hexavalent chromium or decrease it to its trivalent form, which is then immobilized or separated. Because they may combine surface binding, electrostatic interaction, ion exchange, complexation, and in some cases Cr(VI) reduction, biological and biosorptive approaches become attractive [1,2]. Chromium contamination of environments continue to be a serious problem because chromium occurs either as Cr(III) or Cr(VI), these two forms of chromium greatly differ in toxicity mobility, and environmental behaviour. Cr(VI) is highly soluble, highly mobile, and hazardous because it ability to access biological systems and induce oxidative stress. Conversely, Cr(III) is generally less mobile and less toxic. Hexavalent chromium is primarily used in many industries, including stainless steel, textile, chemical manufacturing, metallurgy, electroplating, printing, tanning, dye, and leather, as well as in wood preservation processes. Many of these companies release chromium-containing wastewater straight into water bodies without adequate treatment, or sometimes without treatment at all. This results in pollution and degradation of the ecosystem [2,3].

Chemical precipitation, membrane filtration, Ion exchange, adsorption with activated carbon, and evaporation are some of the conventional techniques used to remove heavy metals from solutions. When heavy metal concentrations exceed acceptable limits, however, many of these technologies either fail or become prohibitively expensive. These methods add another disposal issue to the list due to their high initial investment, limited efficiency, significant waste output, and high running and capital expenses. They also fail to adequately recover heavy metals. As a result, biosorption has drawn interest as a low-cost and perhaps

sustainable substitute, particularly in situations where cheap biological leftovers or agro-industrial wastes are accessible. The ability of biological materials to bind metal ions or oxyanions through functional groups on their surfaces, such as hydroxyl, carboxyl, phosphate, amine, amide, and sulfur-containing groups, is the foundation of biosorption [4,3]. Because fungal cell walls include chitin, glucans, proteins, lipids, and polysaccharides that offer several metal-binding sites, fungal biomass is especially well-suited as a biosorbent. Because it doesn't require food input, is less susceptible to metal toxicity, and may be utilized in a wider range of physicochemical circumstances, dead or wasted fungal biomass is frequently preferred over active biomass. Dead fungal biomass, such as Aspergillus niger and other fungal materials, can extract Cr(VI) from aqueous solutions, according to a number of studies. Because protonation of biomass functional groups increases the interaction between the fungal surface and negatively charged Cr(VI) species, removal is frequently preferred in acidic environments [5–7].

Several experimental factors, including pH, contact time, biomass dose, initial chromium concentration, particle size, pretreatment method, temperature, and the presence of competing ions, controlled the biosorption of chromium by fungal biomass. Chromium uptake is usually improved by pretreatment of fungal biomass, which results in modification of functional groups involved in binding and increased surface accessibility. For example, chemically pretreated Aspergillus niger and immobilised fungal biomass have been tested in both column batch systems, demonstrating the practical relevance of fungal biosorbents beyond simple screening experiments [5,8]. However, batch studies alone are not sufficient. Further work is required for process development using regeneration tests, desorption studies, continuous-flow columns, and real wastewater matrices.vAlthough it is more accurately described as a synthetic hydrogel or composite matrix rather than a natural biomass, polyacrylamide can be considered a useful polymer-assisted biosorbent platform. Its adsorption potential arises from high water uptake, amide groups, flexible porous structure, and the possibility of partial hydrolysis to introduce carboxylate groups with stronger affinity for metal ions. Polyacrylamide hydrogels that have been crosslinked have been reported to remove Pb(II), Cu(II), and Cd(II), with pH, temperature, and initial metal concentration affecting the adsorption process [9].

The material becomes more biosorbent-like because amino, hydroxyl, amide, and carboxylate groups can contribute to chelation, ion exchange, and electrostatic binding when polyacrylamide is combined with biomass-derived polymers. For example, removal of Cu(II), Pb(II), and Hg(II) by hydrolysed polyacrylamide-chitosan beads with bead size suitable for column application [10]. EDTA-functionalized chitosan/polyacrylamide double-network hydrogel also showed strong heavy-metal binding due to additional chelating sites [11]. Improved Co(II) and Ni(II) adsorption by mineral hybridization have been demonstrated by Polyacrylamide–montmorillonite nanocomposites [12]. Thus, polyacrylamide is best positioned as a biosorbent composites for functional support, especially when blended with chelating groups, clay or biomass. Biosorption is a prosperous alternative for removing chromium because it can use inexpensive waste biomass, it can operate relatively under simple conditions, and treatment systems with less energy requirements. However, careful evaluation of its practical application is necessary. A reliable chromium biosorption study should include kinetic analysis, equilibrium modelling, thermodynamic assessment, adsorbent characterisation, regeneration performance, and fixed-bed validation where applicable. In the present work, we evaluate chromium adsorption onto fungal biomass using different isotherm models. Multiobjective Optimization on the Basis of Ratio Analysis method was used for model performance identification and ranking of the most suitable adsorption model.

METHODS

Data acquisition and fitting

The freeware Webplotdigitizer 2.5 was used to digitize Figure 3 data from a previously published work [5]. The program's digitizing capabilities have received praise for their dependability [13]. The data was then subjected to nonlinear regression using Curve-Expert Professional (Version 2.6.5, copyright Daniel Hyams), a curve fitting application, while the implicit equation of the Fowler-Guggenheim model was solved using the MATLAB software suite (Mathworks, Massachusetts, USA).

Isotherms

The isothermal models utilized in this study (**Table 1**) is limited to three-parameter models to prevent overfitting and shown below.

Statistical analysis

The following statistical discriminatory or error function tests were used in this investigation: Bias Factor (BF), Accuracy Factor (AF) [14], root-mean-squared error (RMSE), adjusted coefficient of determination (R^2) [15], corrected Akaike Information Criterion (AICc) [16,17], Marquardt's percent standard deviation (MPSD) [18–20], and Bayesian Information Criterion [21]. Obi and Pdi are the expected and observed values, n is the total number of observations, and p is the total number of model parameters [22].

RMSE was calculated using the following formula;

$$RMSE = \sqrt{\frac{\sum_{i=1}^{n}(Pd_i - Ob_i)^2}{n-p}} \quad \text{(Eqn. 1)}$$

BF and AF were calculated using the following formula;

$$Bias\ factor = 10\left(\sum_{i=1}^{n} log\frac{(Pd_i/Ob_i)}{n}\right) \quad \text{(Eqn. 2)}$$

$$Accuracy\ factor = 10\left(\sum_{i=1}^{n} log\frac{|(Pd_i/Ob_i)|}{n}\right) \quad \text{(Eqn. 3)}$$

AICc was calculated using the following formula;

$$AICc = 2p + nln\left(\frac{RSS}{n}\right) + \frac{2(p+1)+2(p+2)}{n-p-2} \quad \text{(Eqn. 4)}$$

BIC was calculated using the following formula;

$$BIC = n\ln\left(\frac{RSS}{n}\right) + k\ln(n) \quad \text{(Eqn. 5)}$$

HQC was calculated using the following formula;

$$HQC = nIn\left(\frac{RSS}{n}\right) + 2k\ln(\ln n) \quad \text{(Eqn. 6)}$$

Adjusted coefficient of determination (R^2) was calculated using the following formula;

$$Adjusted\ (R^2) = 1 - \frac{RMS}{S_Y^2} \quad \text{(Eqn. 7)}$$

$$Adjusted\ (R^2) = 1 - \frac{(1-R^2)(n-1)}{(n-p-1)} \quad \text{(Eqn. 8)}$$

MPSD was calculated using the following formula;

$$MPSD = 100\sqrt{\frac{1}{n-p}\sum_{i=1}^{n}\left(\frac{Ob_i - Pd_i}{Ob_i}\right)^2} \quad \text{(Eqn. 9)}$$

Table 1. Mathematical models in the remodelling data.

Isotherm	*p*	Formula	Ref.
Henry's law	1	$q_e = HC_e$	[23]
Langmuir	2	$q_e = \frac{q_{mL} b_L C_e}{1 + b_L C_e}$	[24]
Jovanovic	2	$q_e = q_{mJ}(1 - e^{-K_J C_e})$	[25]
Freundlich	2	$q_e = K_F C_e^{\frac{1}{n_F}}$	[26]
Dubinin-Radushkevich[a]	2	Incorrect form $q_e = q_{mDR} exp\left\{-K_{DR}\left[RTln\left(1 + \frac{1}{C_e}\right)\right]^2\right\}$ correct form $q_e = q_{mDR} exp\left\{-K_{DR}\left[RTln\left(\left(\frac{C_s}{C_e}\right)\right)\right]^2\right\}$	[27,28] [29,30]
Koble-Corrigan[c]	3	$q_e = \frac{AC_e^n}{1 + BC_e^n}$	[31]
Temkin[a]	3	$q_e = \frac{RT}{b_T}\{ln(a_T C_e)\}$	[32,33]
Redlich-Peterson	3	$q_e = \frac{K_{RP1} C_e}{1 + K_{RP2} C_e^{\beta_{RP}}}$	[34]
Sips[c]	3	$q_e = \frac{K_s q_{mS} C_e^{\frac{1}{n_S}}}{1 + K_s C_e^{\frac{1}{n_S}}}$	[35]
Toth	3	$q_e = \frac{q_{mT} C_e}{\left(K_T + C_e^{n_T}\right)^{n_T}}$	[36]
Hill[c]	3	$q_e = \frac{q_{mH} C_e^{n_H}}{K_H + C_e^{n_H}}$	[37]
BET	3	$q_e = \frac{q_{mBET} \alpha_{BET} C_e}{(1 - \beta_{BET} C_e)(1 - \beta_{BET} C_e + \alpha_{BET} C_e)}$	[38]
Vieth-Sladek	3	$q_e = \frac{q_{mVS} b_{VS} C_e}{(1 + b_{VS} C_e)^{n_{VS}}}$	[39]
Brouers–Sotolongo	3	$q_e = q_{mBS}\left[1 - \left(1 + (0.5)\left(\frac{t}{\tau}\right)^{\alpha}\right)^{-2}\right]$	[40–42]
Fritz-Schlunder-III	3	$q_e = \frac{q_{mFS} K_{FS} C_e}{1 + K_{FS} C_e^{n_{FS}}}$	[43]
Fowler-Guggenheim[a,b]	3	$q_e = q_{mFG} \frac{K_L C_e e^{\frac{\alpha q_e}{q_{mFG}}}}{1 + K_L C_e e^{\frac{\alpha q_e}{q_{mFG}}}}$	[44]
Moreau	3	$q_e = q_{mM} \frac{bC_e + lb^2 {C_e}^2}{1 + 2bC_e + lb^2 {C_e}^2}$	[45]
Unilan	3	$q_e = \frac{q_{mU}}{2b_U} ln\left(\frac{a_U + C_e e^{b_U}}{a_U + C_e e^{-b_U}}\right)$	

Note
[a]Models that include ln(C_e), implicit equation or any logarithmic function involving C_e will fail or produce NaN (undefined) results when C_e = 0. Therefore, data points where C_e = 0 should be excluded from the analysis.
[b]Implicit equation or function.
[c]The Hill, Liu (omitted), Sips, and Koble–Corrigan isotherm models will be presented in their traditional forms to preserve their historical context and conceptual distinctions, despite their underlying equality [46,47].

Application of Multiobjective Optimization by Ratio Analysis (MOORA) in Modeling

For multi-criteria decision-making (MCDM) in the modeling exercise, Multiobjective Optimization by Ratio Analysis (MOORA) was used since the best models frequently exhibit a combination of error function superiority. This method makes it easier to choose the best model by analyzing several performance parameters at once [48,49]. The first stage in the process is to normalize the decision matrix so that various performance indicators may be compared. Next, the choice matrix underwent normalization. Since these metrics could have different magnitudes and units, normalization must be done using the following formula:

$$X'_{ij} = \frac{x_{ij}}{\sqrt{\sum_{i=1}^{n} x_{ij}^2}} \qquad \text{(Eqn. 10)}$$

Where X_{ij} is the original value of the j^{th} metric for the i^{th} model, and X^i_{ij} is the normalized value.

Ratio System Analysis

A ratio system approach was then used to aggregate the normalized values. The following formula was used to deduct non-beneficial criteria (the remaining error functions) or those that should be minimized from advantageous criteria (those that should be maximized, adjR^2.

$$Y_i = \sum_{beneficial} X'_{ij} - \sum_{non-beneficial} X'_{ij} \qquad \text{(Eqn. 11)}$$

Where Y_i is the final score for the i^{th} model

It is advised to include weighted ratios in the analysis when some criteria were judged to be more important than others. Since there is currently no consensus in the literature over which of the error functions mentioned above should take precedence over the others, the recommendation to incorporate Weighted Ratios is not implemented. Ranking models according to their combined performance scores is the last stage. Better performance was reflected by higher scores. According to the specified decision

criteria, the model with the highest value was deemed the best. This approach made it possible to compare kinetic models objectively and methodically, making it easier to determine which model performed the best while taking into account several performance criteria at once.

RESULTS AND DISCUSSION

Nonlinear regression was used to apply a number of models to the equilibrium data of [5]. The publication's data was transformed from the initial concentration to the standard C_e.

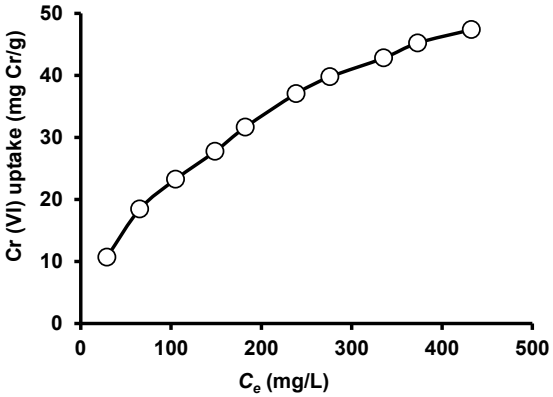

Fig. 1. Equilibrium adsorption of chromium to fungal biomass raw data extracted using Webplot.

The fungal biomass's uptake of Cr(VI) increased as the equilibrium concentration, C_e, increased, according to the experimental isotherm profile (**Fig. 1**). q_e increased dramatically from about 11 to 23 mg Cr/g at low C_e (below 100 mg/L), suggesting a high initial affinity between Cr(VI) species and easily accessible binding sites on the surface of the fungal biomass. At the highest tested concentration, q_e grew more slowly as C_e climbed and reached about 47 mg Cr/g (at C_e approximately 430 mg/L). A fully horizontal plateau was not clearly created, despite the curve's inclination toward saturation, indicating that the true maximum adsorption capacity might not have been entirely reached within the examined range.

The adsorption behavior was better explained by multi-parameter models than by more straightforward, conventional equations, according to nonlinear isotherm fitting and error function analysis (**Table 2**). Based on the MOORA multi-criteria decision-making method (**Table 3**), the Brouers–Sotolongo model was ranked as the best fit for the experimental data with a top score of 0.60. It was followed closely by the Sips and Hill models, which tied for the second position with an identical MOORA score of 0.56. The Redlich-Peterson (rank 4, score 0.53) and Fritz-Schlunder III (rank 5, score 0.37) models rounded out the top five, while the Toth model placed sixth (score 0.36). The superior performance of the Brouers–Sotolongo, Sips, Hill, and Redlich-Peterson models, all achieving ideal coefficients of determination (R^2 = 1.00) and low error metrics (e.g., Brouers–Sotolongo achieved an RMSE of 0.555, AICc of 6.641, and adR^2 of 0.998), strongly suggests adsorption occurs on a heterogeneous fungal biomass surface with a variety of distinct binding groups.

These typically include hydroxyl, carboxyl, phosphate, amine, and amide functionalities [5,6,8,50]. Conversely, traditional two-parameter models like the Freundlich and Langmuir performed worse, ranking 7th (score 0.20) and 8th (score 0.18), respectively. Other models like Temkin, Jovanovic, Koble-Carrigan, and BET showed progressively lower or negative MOORA scores, with Fowler-Guggenheim ranking last (rank 17, score -1.82). Consequently, even though the experimental curve indicated a strong tendency toward saturation, an ideal homogeneous monolayer model (Langmuir) was unable to adequately explain the complex biosorption process. Overall, the MOORA ranking firmly establishes the Brouers–Sotolongo model as the optimal mathematical description for Cr(VI) biosorption by this fungal biomass.

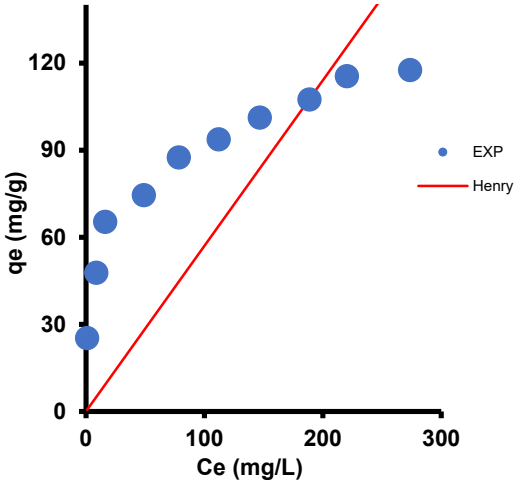

Fig. 2. Cr (VI) adsorption onto fungal biomass modelled using the Henry model.

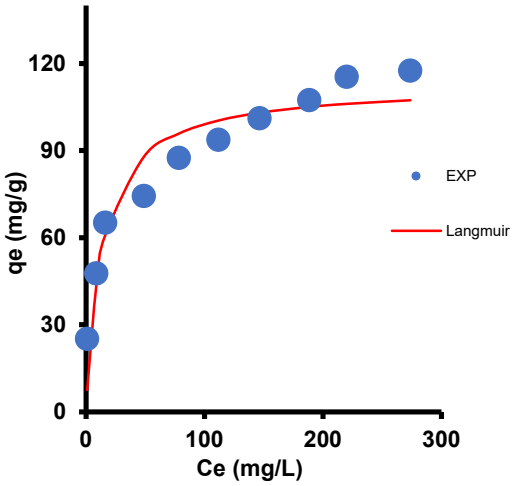

Fig. 3. Cr (VI) adsorption onto fungal biomass modelled using the Langmuir isotherm model.

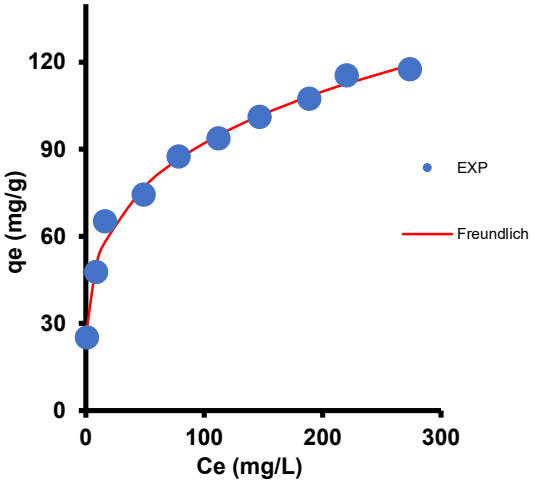

Fig. 4. Cr (VI) adsorption onto fungal biomass modelled using the Freundlich isotherm model.

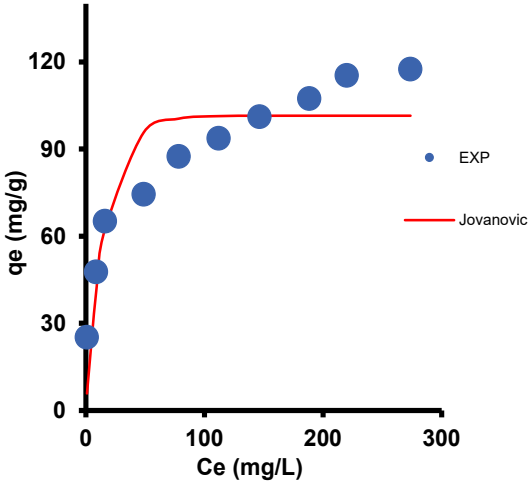

Fig. 7. Cr (VI) adsorption onto fungal biomass modelled using the Jovanovic isotherm model.

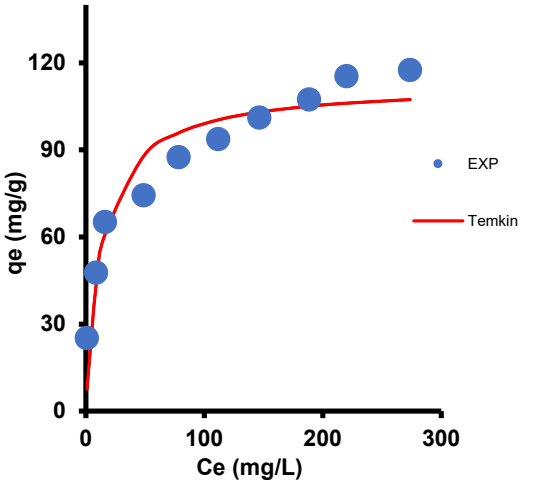

Fig. 5. Cr (VI) adsorption onto fungal biomass modelled using the Temkin isotherm model.

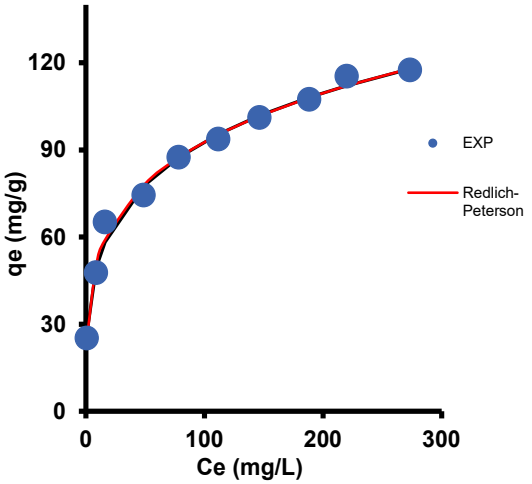

Fig. 8. Cr (VI) adsorption onto fungal biomass modelled using the Redlich-Peterson isotherm model.

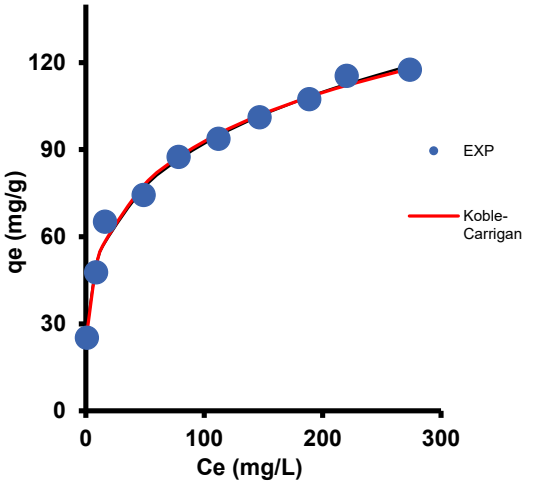

Fig. 6. Cr (VI) adsorption onto fungal biomass modelled using the Koble-Corrigan isotherm model.

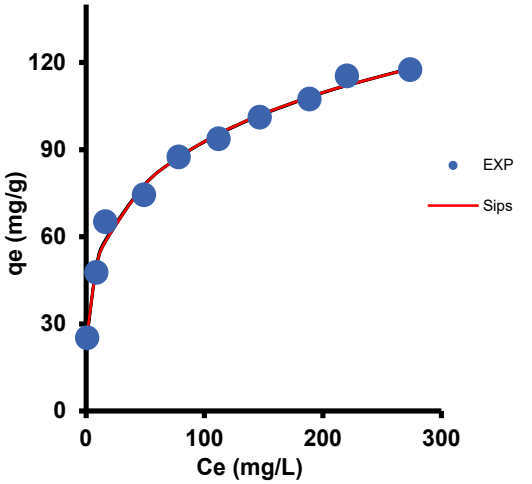

Fig. 9. Cr (VI) adsorption onto fungal biomass modelled using the Sips isotherm model.

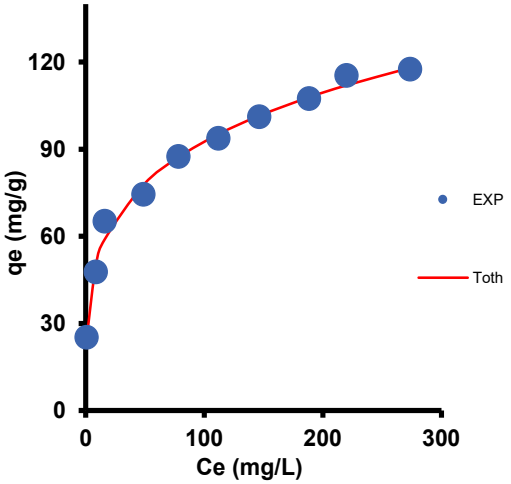

Fig. 10. Cr (VI) adsorption onto fungal biomass modelled using the Toth isotherm model.

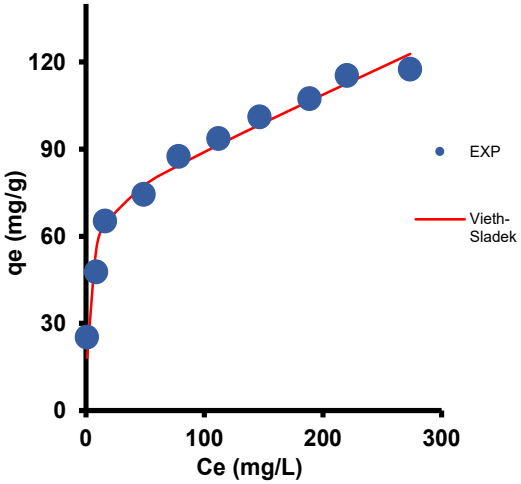

Fig. 13. Cr (VI) adsorption onto fungal biomass modelled using the Vieth-Sladek isotherm model.

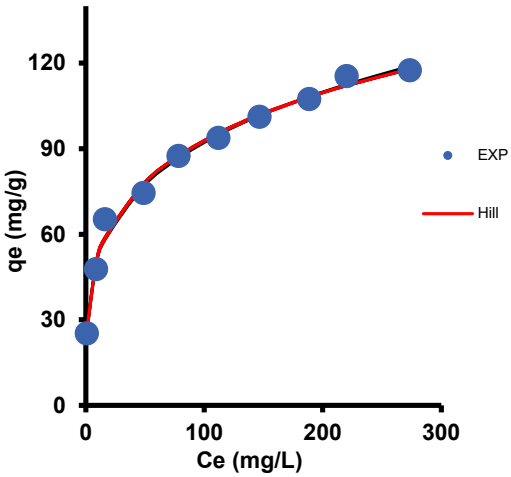

Fig. 11. Cr (VI) adsorption onto fungal biomass modelled using the Hill isotherm model.

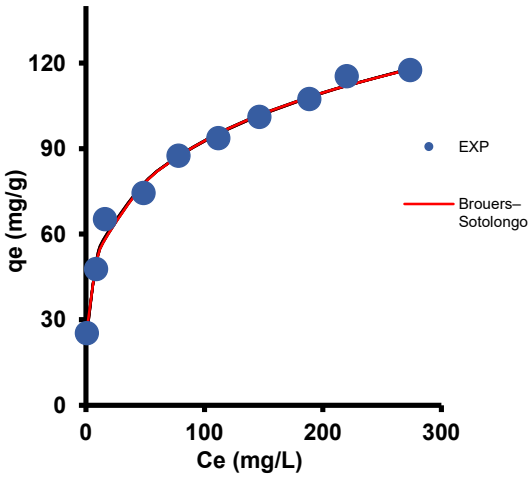

Fig. 14. Cr (VI) adsorption onto fungal biomass modelled using the Brouers-Sotolongo isotherm model.

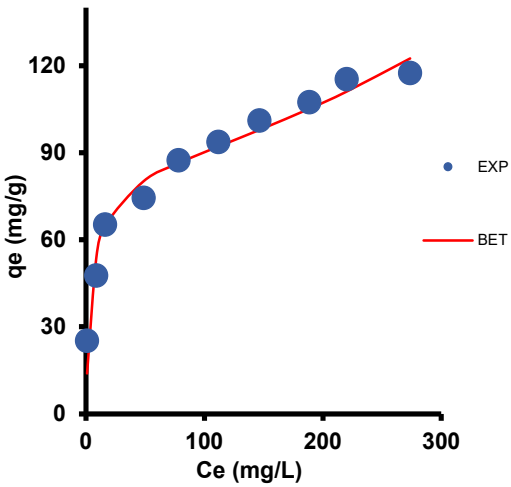

Fig. 12. Cr (VI) adsorption onto fungal biomass modelled using the BET isotherm model.

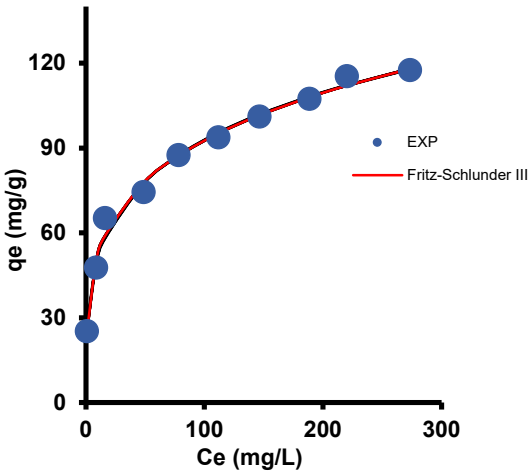

Fig. 15. Cr (VI) adsorption onto fungal biomass modelled using the Fritz-Schlunder III isotherm model.

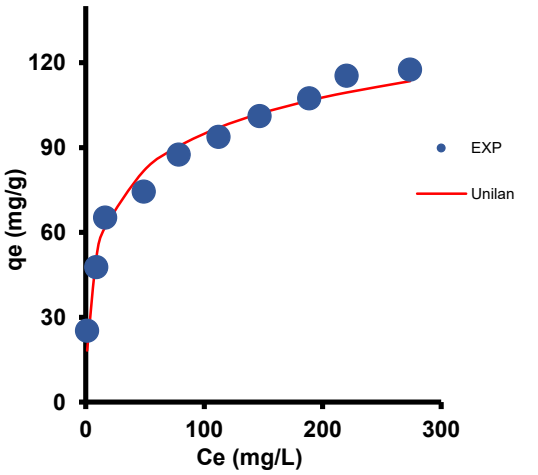

Fig. 16. Cr (VI) adsorption onto fungal biomass modelled using the Unilan isotherm model.

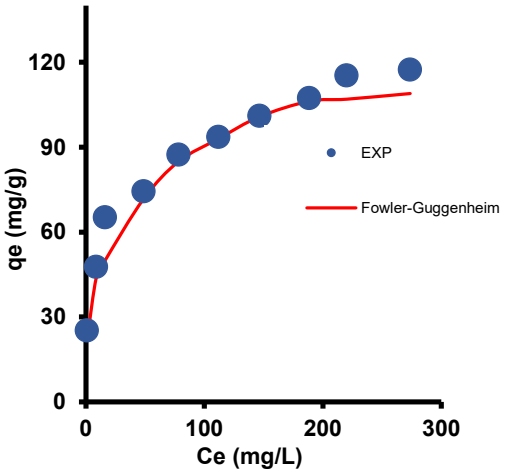

Fig. 18. Cr (VI) adsorption onto fungal biomass modelled using the Fowler-Guggenheim isotherm model.

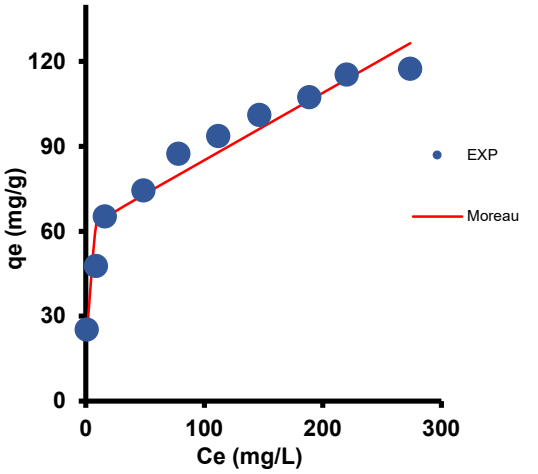

Fig. 17. Cr (VI) adsorption onto fungal biomass modelled using the Moreau isotherm model.

Table 2. Error function analysis for the fitting of the isotherm of Cr (VI) adsorption onto fungal biomass.

Model	RPSD	MSE	^{2}	adR^2	AICc	BIC	HQC	AF	BF
Henry	97.32	.524	.83	803	7.022	1.61	0.98	.982	.087
Langmuir	5.58	.151	.99	991	4.575	.18	.91	.001	.007
Freundlich	7.34	.924	.99	993	0.198	.80	0.47	.996	.011
Temkin	9.12	.230	.99	989	2.575	.48	.58	.001	.007
Hoble-Carrigan	15.29	.536	.96	95	0.687	0.08	.1.35	.998	.005
Ivanovic	0.56	.610	.99	982	1.289	1.89	0.63	.004	.012
Redlich-Peterson	.77	.629	.00	997	.161	6.93	7.84	.998	.006
Hips	1.51	.573	.00	997	.294	7.80	0.70	.998	.006
Both	.72	.827	.00	995	4.636	0.46	2.36	.997	.009
Hill	1.51	.573	.00	997	.294	7.80	0.70	.998	.006
BET	73.39	.866	.00	994	5.551	.46	.44	.998	.008
Dieth-Sladek	.94	.319	.84	754	0.804	5.71	3.81	.992	.066
Frouers–Sotolongo	1.16	.555	.00	998	.641	6.45	0.35	.998	.005
Fritz-Schlunder III	.78	.813	.00	995	4.301	0.79	2.69	.996	.009
Hanilan	9.61	.338	.82	737	0.850	5.76	3.85	.976	.091
Fowler-Guggenheim	4.58	0.317	.85	774	5.108	0.02	3.11	.122	.122
Moreau	9.34	.021	.98	967	2.504	7.41	5.51	.973	.973

Note:
RMSE Root mean Square Error
adR^2 Adjusted Coefficient of determination
p no of parameters
AF Accuracy factor
BF Bias factor
BIC Bayesian Information Criterion
AICc Adjusted Akaike Information Criterion
HQC Hannan–Quinn information criterion

Cr(VI) uptake by polyacrylamide-immobilized fungal biomass rose gradually with equilibrium concentration, according to the isotherm profile displayed. At higher C_e values, there was a tendency toward plateau development. This trend shows that as the concentration of Cr(VI) rose, the available binding sites were progressively occupied, and the system was becoming close to saturation within the range under study. The curve does not seem to be precisely linear, indicating that Henry-type behavior or straightforward partitioning is insufficient. Rather, heterogeneous surface binding and finite-capacity adsorption are more in line with the concave downhill shape.

Table 3. Ranking of isothermal models based on MOORA.

No	Model	MOORA Score	Rank
1	Brouers–Sotolongo	0.60	1
2	Sips	0.56	2
3	Hill	0.56	2
4	Redlich-Peterson	0.53	4
5	Fritz-Schlunder III	0.37	5
6	Toth	0.36	6
7	Freundlich	0.20	7
8	Langmuir	0.18	8
9	Temkin	0.06	9
10	Jovanovic	-0.01	10
11	Koble-Carrigan	-0.04	11
12	BET	-0.05	12
13	Moreau	-0.30	13
14	Vieth-Sladek	-1.51	14
15	Unilan	-1.57	15
16	Henry	-1.72	16
17	Fowler-Guggenheim	-1.82	17

Table 4. Isothermal models' constants for Cr (VI) adsorption onto fungal biomass immobilized on polyacrylamide.

Model	p	Unit	Value	(95% confidence interval)
Langmuir	q_{mL}	mg g^{-1}	68.05	61.89 to 75.11
	b_L	L mg^{-1}	0.01	0.004 to 0.006
Brouers-Sotolongo	q_{mB}	mg g^{-1}	76.33	51.29 to 101.37
	s	$mg^{-1/nBS}$ $L^{1/nBS}$	0.01	0.01 to 0.02
	K_{BS}	dimensionless	1.44	1.23 to 1.65
	n_{BS}	s		
Sips	q_{mS}	mg g^{-1}	115.9	61.22 to 170.66
	K_S	$(L\ mg^{-1})^{ns}$	8	0.004 to 0.015
	n_S	Dimensionless	0.009	1.14 to 1.65
			1.39	

This interpretation is further supported by the MOORA-based rating. Redlich-Peterson, Fritz-Schlunder III, and Toth all outperformed the traditional Langmuir and Freundlich equations, with the Brouers-Sotolongo model coming in first, followed by the Sips and Hill models. This implies that rather than being explained by a straightforward homogeneous monolayer assumption, Cr(VI) adsorption onto the immobilized fungal biomass was better explained by models that take into consideration surface heterogeneity, non-ideal binding, and potential site-energy distribution. Because the biosorbent surface comprises chemically various functional groups, such as hydroxyl, carboxyl, phosphate, amine, and amide groups, which may contribute variably to Cr(VI) binding, the supremacy of Brouers–Sotolongo is especially appropriate for fungal biomass.

The Langmuir model offered a helpful finite-capacity estimate despite not being the top-ranked model. A corrected Langmuir analysis yielded a q_{mL} value of 68.05 mg/g. This discrepancy suggests that model form, dataset size, or correction technique may have an impact on parameter estimation. Consequently, rather than serving as conclusive evidence of perfect monolayer adsorption, the Langmuir capacity should be viewed as an operational approximation. Overall, the isotherm behavior indicates that fungal functional groups most likely supplied the primary binding sites necessary for Cr(VI) biosorption, whereas polyacrylamide immobilization offered a stable matrix for fungal biomass. In the original study, it relies exclusively on the Freundlich isotherm. This remodelling exercise addresses a critical limitation where the Freundlich model is known to be inherently incapable of predicting a maximum adsorption capacity (q_m). In the original work, the authors reported maximum capacities of 119.2 mg/g for the free biomass and 45.56 mg/g for the polyacrylamide-immobilized biomass at a Cr(VI) concentration of 500 mg/L. However, they did not disclose the methodology or mathematical models used to derive these values.

Brouers-Sotolongo

Using the ideas of classical models, the Brouers-Sotolongo (BS) model is an isotherm model that explains the adsorption processes on heterogeneous surfaces. New parameters were introduced to the BS model to characterize the complexity and diversity of active sites on the adsorbent material. The BS model provides a generalized approach to characterizing adsorption isotherms. The model's superiority has been shown in numerous applications.

The BS model was determined to be the best fit for the adsorption data in a study on the biosorption of yellow tartrazine dye by the agro-industrial wastes sugarcane bagasse and rice husk [51]. The BS model fit the experimental data quite well, according to other studies that used models for metal sorption on soils, such as the Brouers-Sotolongo, Sips, Hill, and Langmuir-Freundlich models [52]. In a recent study on the adsorption of mercury (II) ions (Hg^{2+}) onto a new porous organic polymer, BS proved to be the most effective model [53]. In a different study on eliminating Gram-negative enteric bacteria with a hybrid clay composite that has been surface-modified with chitosan, the BS model was also the most effective model [54].

A combination of the Freundlich and Langmuir isotherms is the Sips model. Sips is used to predict adsorption systems that are heterogeneous. The approach overcomes the modelling disadvantage of Freundlich isotherm associated with rise in solute concentration. The model effectively reduces to the Freundlich isotherm at low solute concentrations, while the equation simplifies to the Langmuir model of monolayer sorption capacity at high solute concentrations [55]. Biosorption isotherm data have been successfully modeled using the Sips model [56–61].

With a 95 percent confidence interval of 61.89 to 75.11 mg/g, the Langmuir parameters estimated a maximum adsorption capacity, q_{mL}, of 68.05 mg/g. The closeness of this estimated value to the maximum observed experimental values indicates that a physically plausible estimation of the upper adsorption capacity within the studied concentration range is provided by the Langmuir model. Additionally, the model shows a 95 percent confidence interval of 0.004 to 0.006 L/mg and a Langmuir affinity constant, q_{mL}, of 0.01 L/mg, suggesting a specific level of affinity between the surface of the fungal biomass and hexavalent chromium species. Though a reasonable physical q_{mL} value was obtained, the capacity estimate alone should not lead to the conclusion that the Langmuir model is the best model. According to the MOORA ranking, the Brouers-Sotolongo (BS) model gave the best overall fit, followed by Sips. This implies that models that account for non-ideal adsorption behaviour and surface heterogeneity describe complete equilibrium better. This

is expected because of the various functional groups present in fungi that are known for metal binding. The computational efficiency and simplicity associated with MOORA has eliminated distance computations and the need for intricate pairwise comparisons. Performance ratings across criteria are also standardized. Through the management of criteria with varying units and scales via structured normalization, MOORA can facilitate clear and swift assessment. In various model ranking tasks, MCDM has been widely and successfully utilized, including the assessment of Software Reliability Growth Models (SRGMs) [62], however, there is limited application in model selection in adsorption [47].

The datasets are a notable limitation of nonlinear modeling (like the eight data points utilized in this study), which may not adequately represent true adsorption behavior as previously stated. Instead of recognizing authentic adsorption patterns, the chances of recording random noise increase with an insufficient dataset. Unreliable parameter estimation of adsorption models, overfitting, and incorrect interpretation of adsorption mechanisms are some of the problems associated with limited data in nonlinear regression. Wide confidence intervals and reduced statistical power are also caused by limited datasets. To address these challenges, resampling techniques such as bootstrapping, Monte Carlo simulations, and sensitivity analysis can be employed. Robustness of the model will be enhanced, giving more insight into adsorption behaviour. Thereby overcoming the listed changes [63].

Langmuir isotherm

The Langmuir isotherm characterizes monolayer adsorption of an adsorbate onto a homogeneous adsorbent surface, which only happens when the adsorbent has a uniform structure. Every adsorption site in the model has the same energy and is similar [24]. Although the isotherm model and Henry's law are different, their underlying ideas are similar. The concept of monolayer coverage is reinforced by the theory that once a single layer of adsorbate molecules completely covers the surface, no more adsorption can take place at those locations [64]. Several studies have reported successful utilization of the Langmuir model as the best model for equilibrium adsorption isotherms [65–78].

CONCLUSION

Nonlinear modelling demonstrated that Cr(VI) adsorption onto polyacrylamide-immobilized fungal biomass follows a concave downward isotherm profile, indicating a heterogeneous biosorption process rather than simple Henry-type partitioning. While the Langmuir model estimated a maximum adsorption capacity of 68.05 mg/g (95% confidence interval: 61.89 to 75.11 mg/g) as the curve approached an apparent plateau at higher equilibrium concentrations (C_e), MOORA ranking identified the Brouers–Sotolongo model as the best-performing overall model. The Brouers–Sotolongo model yielded a maximum adsorption capacity of 76.33 mg/g (95% confidence interval: 51.29 to 101.37 mg/g). This superior fit highlights that the full equilibrium profile is better explained by models accounting for structural heterogeneity, which aligns with the complex surface chemistry of the immobilized fungal biomass. Overall, this study demonstrates the strong potential of polyacrylamide-immobilized fungal biomass for the remediation of toxic Cr(VI) from aquatic systems. Although nonlinear regression combined with MOORA ranking significantly improved isotherm evaluation, future work should incorporate broader equilibrium data and advanced parameter validation to further optimize this biosorptive system.

DECLARATION OF COMPETING INTEREST

The authors declare no competing financial interests or personal relationships.

ACKNOWLEDGEMENT

This research is funded by Universiti Putra Malaysia Inisiatif Putra Siswazah Grant, with a reference to GP-IPS/2024/GP-IPS/9785100 and the essential facilities were provided by UDRP Bioremediation and Conservation, Universiti Putra Malaysia.

AUTHORS' CONTRIBUTION

I.H. contributed to conceptualization, methodology, investigation, and writing the original draft. M.E.K. was involved in methodology, investigation, and data analysis. N.A.Y. contributed to investigation, resources, and data collection. A.A.B. participated in investigation, resources, and data collection. M.Y.S. contributed to methodology, validation, and writing review and editing.

DATA AVAILABILITY STATEMENT

Data available on request

AI USAGE DECLARATION

During the preparation of this work, the authors used generative AI technologies solely for language editing and refinement. All of the authors reviewed and edited the content. The authors take full responsibility for the final content of the publication.

REFERENCES

1. Srinath T, Verma T, Ramteke P, Garg S. Chromium (VI) biosorption and bioaccumulation by chromate resistant bacteria. Chemosphere 2002;48:427–35
2. Ahemad M. Bacterial mechanisms for Cr (VI) resistance and reduction: an overview and recent advances. Folia Microbiol. (Praha) 2014;59:321–32
3. Pandey K, Saharan BS, Kumar R, Jabborova D, Duhan JS. Modern-day green strategies for the removal of chromium from wastewater. J. Xenobiotics 2024;14:1670–96. https://doi.org/10.3390/jox14040089
4. Ullah I, Nadeem R, Iqbal M, Manzoor Q. Biosorption of chromium onto native and immobilized sugarcane bagasse waste biomass. Ecol. Eng. 2013;60:99–107. https://doi.org/10.1016/j.ecoleng.2013.07.028
5. Bai RS, Abraham TE. Studies on chromium(VI) adsorption–desorption using immobilized fungal biomass. Bioresour. Technol. 2003;87:17–26. https://doi.org/10.1016/S0960-8524(02)00222-5
6. Park D, Yun Y-S, Park JM. Use of dead fungal biomass for the detoxification of hexavalent chromium: screening and kinetics. Process Biochem. 2005;40:2559–65. https://doi.org/10.1016/j.procbio.2004.12.002
7. Khambhaty Y, Mody K, Basha S, Jha B. Biosorption of Cr(VI) onto marine Aspergillus niger: experimental studies and pseudo-second order kinetics. World J. Microbiol. Biotechnol. 2009;25:1413–21. https://doi.org/10.1007/s11274-009-0028-0
8. Mungasavalli DP, Viraraghavan T, Jin Y-C. Biosorption of chromium from aqueous solutions by pretreated *Aspergillus niger*: Batch and column studies. Colloids Surf. Physicochem. Eng. Asp. 2007;301:214–23. https://doi.org/10.1016/j.colsurfa.2006.12.060
9. Lebkiri I, Abbou B, Kadiri L, Ouass A, Essaadaoui Y, Ouaddari H, et al. Polyacrylamide hydrogel an effective adsorbent for the removal of heavy metal from aqueous solution: isotherm, kinetic, and thermodynamic studies. Russ. J. Phys. Chem. A 2022;96:1484-92. https://doi.org/10.1134/S0036024422070159
10. Cao J, Tan Y, Che Y, Xin H. Novel complex gel beads composed of hydrolyzed polyacrylamide and chitosan: An effective adsorbent

for the removal of heavy metal from aqueous solution. Bioresour. Technol. 2010;101:2558-61. https://doi.org/10.1016/j.biortech.2009.10.069
11. Ma J, Zhou G, Chu L, Liu Y, Liu C, Luo S, et al. Efficient removal of heavy metal ions with an EDTA functionalized chitosan/polyacrylamide double network hydrogel. ACS Sustain. Chem. Eng. 2017;5:843-51. https://doi.org/10.1021/acssuschemeng.6b02181
12. Moreno-Sader K, García-Padilla A, Realpe A, Acevedo-Morantes M, Soares JB. Removal of heavy metal water pollutants (Co2+ and Ni2+) using polyacrylamide/sodium montmorillonite (PAM/Na-MMT) nanocomposites. ACS Omega 2019;4:10834-44. https://doi.org/10.1021/acsomega.9b00981
13. Khare KS, Phelan FR. Quantitative Comparison of Atomistic Simulations with Experiment for a Cross-Linked Epoxy: A Specific Volume-Cooling Rate Analysis. Macromolecules 2018;51:564-75. https://doi.org/10.1021/acs.macromol.7b01303
14. Ross T. Indices for performance evaluation of predictive models in food microbiology. J. Appl. Bacteriol. 1996;81:501-8. https://doi.org/10.1111/j.1365-2672.1996.tb01946.x15.
15. Ezekiel M. The Sampling Variability of Linear and Curvilinear Regressions: A First Approximation to the Reliability of the Results Secured by the Graphic "Successive Approximation" Method. Ann. Math. Stat. 1930;1:275–333. https://doi.org/10.1214/aoms/1177733062
16. Akaike H. Factor analysis and AIC. Psychometrika 1987;52:317–32. https://doi.org/10.1007/BF02294359
17. Burnham KP, Anderson DR. Model Selection and Multimodel Inference: A Practical Information-Theoretic Approach. 2nd ed. New York: Springer; 2002.
18. Marquardt DW. An algorithm for least-squares estimation of nonlinear parameters. SIAM J. Appl. Math. 1963;11:431–41
19. Seidel A, Gelbin D. On applying the ideal adsorbed solution theory to multicomponent adsorption equilibria of dissolved organic components on activated carbon. Chem. Eng. Sci. 1988;43:79–88. https://doi.org/10.1016/0009-2509(88)87128-8
20. Porter JF, McKay G, Choy KH. The prediction of sorption from a binary mixture of acidic dyes using single- and mixed-isotherm variants of the ideal adsorbed solute theory. Chem. Eng. Sci. 1999;54:5863–85. https://doi.org/10.1016/S0009-2509(99)00178-5
21. Schwarz G. Estimating the Dimension of a Model. Ann. Stat. 1978;6:461–4
22. Motulsky HJ, Ransnas LA. Fitting curves to data using nonlinear regression: a practical and nonmathematical review. FASEB J. Off. Publ. Fed. Am. Soc. Exp. Biol. 1987;1:365–74. https://doi.org/10.1096/fasebj.1.5.3315805
23. Ridha FN, Webley PA. Anomalous Henry's law behavior of nitrogen and carbon dioxide adsorption on alkali-exchanged chabazite zeolites. Sep. Purif. Technol. 2009;67:336–43. https://doi.org/10.1016/j.seppur.2009.03.045
24. Langmuir I. The constitution and fundamental properties of solids and liquids. Part I. Solids. J. Am. Chem. Soc. 1916;38:2221–95. https://doi.org/10.1021/ja02268a002
25. Jovanović DS. Physical adsorption of gases - I: Isotherms for monolayer and multilayer adsorption. Kolloid-Z. Amp Z. Für Polym. 1969;235:1203–13. https://doi.org/10.1007/BF01542530
26. Carmo AM, Hundal LS, Thompson ML. Sorption of hydrophobic organic compounds by soil materials: Application of unit equivalent Freundlich coefficients. Environ. Sci. Technol. 2000;34:4363–9. https://doi.org/10.1021/es000968v
27. Radushkevich LV. Potential theory of sorption and structure of carbons. Zhurnal Fiz. Khimii 1949;23:1410–20
28. Dubinin MM. Modern state of the theory of volume filling of micropore adsorbents during adsorption of gases and steams on carbon adsorbents. Zh Fiz Khim 1965;39:1305–17
29. Mahanty B, Behera SK, Sahoo NK. Misinterpretation of Dubinin–Radushkevich isotherm and its implications on adsorption parameter estimates. Sep. Sci. Technol. 2023;58:1275–82. https://doi.org/10.1080/01496395.2023.2189050
30. Mudhoo A, Pittman CU. The Dubinin-Radushkevich models: Dissecting the *ps*/*p* to *cs*/*c*e replacement in solid-aqueous interfacial adsorption and tracking the validity of E = 8 kJ mol–1 for assigning sorption type. Chem. Eng. Res. Des. 2023;198:370–402. https://doi.org/10.1016/j.cherd.2023.09.020
31. Koble RA, Corrigan TE. Adsorption isotherms for pure hydrocarbons. Ind. Eng. Chem. 1952;44:383–7. https://doi.org/10.1021/ie50506a049
32. Temkin MI, Pyzhev V. Kinetics of ammonia synthesis on promoted iron catalysts. Acta Physicochim USSR 1940;12:327–56
33. Chu KH. Revisiting the Temkin Isotherm: Dimensional Inconsistency and Approximate Forms. Ind. Eng. Chem. Res. 2021. https://doi.org/10.1021/acs.iecr.1c01788
34. Redlich O, Peterson DL. A Useful Adsorption Isotherm. Shell Dev. Co. Emeryv. Calif. 1958;63:1024
35. Sips R. On the structure of a catalyst surface. J. Chem. Phys. 1948;16:490–5. https://doi.org/10.1063/1.1746922
36. Tóth J. Uniform interpretation of gas/solid adsorption. Adv. Colloid Interface Sci. 1995;55:1–239. https://doi.org/10.1016/0001-8686(94)00226-3
37. Hill AV. The possible effects of the aggregation of the molecules of haemoglobin on its dissociation curves. J Physiol 1910;40:iv–vii. https://doi.org/10.1098/rspb.1936.0046
38. Brunauer S, Emmett PH, Teller E. Adsorption of Gases in Multimolecular Layers. J. Am. Chem. Soc. 1938;60:309–19. https://doi.org/10.1021/ja01269a023
39. Vieth WR, Sladek KJ. A model for diffusion in a glassy polymer. J. Colloid Sci. 1965;20:1014–33. https://doi.org/10.1016/0095-8522(65)90071-1
40. Brouers F, Sotolongo O, Marquez F, Pirard JP. Microporous and heterogeneous surface adsorption isotherms arising from Levy distributions. Phys. Stat. Mech. Its Appl. 2005;349:271–82. https://doi.org/10.1016/j.physa.2004.10.032
41. Hamissa AMB, Brouers F, Mahjoub B, Seffen M. Adsorption of Textile Dyes Using Agave Americana (L.) Fibres: Equilibrium and Kinetics Modelling. Adsorpt. Sci. Technol. 2007;25:311–25. https://doi.org/10.1260/026361707783432533
42. Brouers F, Al-Musawi TJ. Brouers-Sotolongo fractal kinetics versus fractional derivative kinetics: A new strategy to analyze the pollutants sorption kinetics in porous materials. J. Hazard. Mater. 2018;350:162–8. https://doi.org/10.1016/j.jhazmat.2018.02.015
43. Fritz W, Schluender EU. Simultaneous adsorption equilibria of organic solutes in dilute aqueous solutions on activated carbon. Chem. Eng. Sci. 1974;29:1279–82. https://doi.org/10.1016/0009-2509(74)80128-4
44. Chu KH, Tan B. Is the Frumkin (Fowler–Guggenheim) adsorption isotherm a two- or three-parameter equation? Colloid Interface Sci. Commun. 2021;45:100519. https://doi.org/10.1016/j.colcom.2021.100519https://doi.org/10.1016/j.colcom.2021.100519
45. Martucci A, Braschi I, Bisio C, Sarti E, Rodeghero E, Bagatin R, et al. Influence of water on the retention of methyl tertiary-butyl ether by high silica ZSM-5 and Y zeolites: A multidisciplinary study on the adsorption from liquid and gas phase. RSC Adv. 2015;5:86997–7006. https://doi.org/10.1039/c5ra15201a
46. Chu KH, Debord J, Harel M, Bollinger J-C. Mirror, Mirror on the Wall, Which Is the Fairest of Them All? Comparing the Hill, Sips, Koble–Corrigan, and Liu Adsorption Isotherms. Ind. Eng. Chem. Res. 2022;61:6781–90. https://doi.org/10.1021/acs.iecr.2c00507
47. Shukor MY. Chitosan–Silica Composite Aerogel for the Adsorption of Cupric Ions: Isothermal Remodeling and MOORA-Based Model Selection. J. Environ. Microbiol. Toxicol. 2024;12:53–62. https://doi.org/10.54987/jemat.v12i2.1026
48. Karel W, Brauers W, Zavadskas E. The MOORA method and its application to privatization in a transition economy. Control Cybern. 2006;35
49. Brauers W. Multi-objective seaport planning by MOORA decision making. Ann. Oper. Res. 2013;206. https://doi.org/10.1007/s10479-013-1314-7
50. Beig S-U-R, Shah SA. Biosorption of Cr (VI) by acid-modified based-waste fungal biomass from Calocybe indica fruiting bodies production. Int. J. Phytoremediation 2023;25:1269–88. https://doi.org/10.1080/15226514.2022.2147145
51. Micheletti DH, Andrade JGS, Porto CE, Barros BCB, Rosa SLF, Sakai OA, et al. Valorization of agro-industrial wastes of sugarcane bagasse and rice husk for biosorption of Yellow Tartrazine dye. An. Acad. Bras. Ciênc. 2024;96:e20231308. https://doi.org/https://doi.org/10.1590/0001-3765202420231308
52. Sipos P. Searching for optimum adsorption curve for metal sorption on soils: comparison of various isotherm models fitted by different

error functions. SN Appl. Sci. 2021;3:387. https://doi.org/10.1007/s42452-021-04383-0
53. Zuo S, Sun Y, Zheng Y, Sun X, Hu J. Efficient selective uptake of Hg(II) using a porous organic polymer rich in N and S atoms. J. Environ. Chem. Eng. 2024;12:111924. https://doi.org/10.1016/j.jece.2024.111924
54. Unuabonah EI, Adebowale KO, Olu-Owolabi BI, Yang LZ, Kong LX. Adsorption of Pb (II) and Cd (II) from aqueous solutions onto sodium tetraborate-modified Kaolinite clay: Equilibrium and thermodynamic studies. Hydrometallurgy 2008;93:1–9. https://doi.org/10.1016/j.hydromet.2008.02.009
55. Sivarajasekar N, Baskar R. Adsorption of basic red 9 onto activated carbon derived from immature cotton seeds: isotherm studies and error analysis. Desalination Water Treat. 2014;52:7743–65. https://doi.org/10.1080/19443994.2013.834518
56. Veličković ZS, Marinković AD, Bajić ZJ, Marković JM, Perić-Grujić AA, Uskokovic PS, et al. Oxidized and ethylenediamine-functionalized multi-walled carbon nanotubes for the separation of low concentration arsenate from water. Sep. Sci. Technol. 2013;48:2047–58. https://doi.org/10.1080/01496395.2013.790446
57. Mondal S, Sinha K, Aikat K, Halder G. Adsorption thermodynamics and kinetics of ranitidine hydrochloride onto superheated steam activated carbon derived from mung bean husk. J. Environ. Chem. Eng. 2015;3:187–95. https://doi.org/10.1016/j.jece.2014.11.021
58. Anirudhan TS, Deepa JR, Christa J. Nanocellulose/nanobentonite composite anchored with multi-carboxyl functional groups as an adsorbent for the effective removal of Cobalt(II) from nuclear industry wastewater samples. J. Colloid Interface Sci. 2016;467:307–20. https://doi.org/10.1016/j.jcis.2016.01.023
59. da Rosa ALD, Carissimi E, Dotto GL, Sander H, Feris LA. Biosorption of rhodamine B dye from dyeing stones effluents using the green microalgae *Chlorella pyrenoidosa*. J. Clean. Prod. 2018;198:1302–10. https://doi.org/10.1016/j.jclepro.2018.07.128
60. Torres-Caban R, Vega-Olivencia CA, Alamo-Nole L, Morales-Irizarry D, Roman-Velazquez F, Mina-Camilde N. Removal of copper from water by adsorption with calcium-alginate/spent-coffee-grounds composite beads. Materials 2019;12:395. https://doi.org/10.3390/ma12030395
61. Zhang M, Zhu L, He C, Xu X, Duan Z, Liu S, et al. Adsorption performance and mechanisms of Pb(II), Cd(II), and Mn(II) removal by a β-cyclodextrin derivative. Environ. Sci. Pollut. Res. 2019;26:5094–110. https://doi.org/10.1007/s11356-018-3989-4
62. Gupta A, Gupta N, Garg R, Kumar R. Evaluation, Selection and Ranking of Software Reliability Growth Models using Multi criteria Decision making Approach. 2018 4th Int. Conf. Comput. Commun. Autom. ICCCA 2018:1–8. https://doi.org/10.1109/CCAA.2018.8777644
63. Lambert RJW, Mytilinaios I, Maitland L, Brown AM. Monte Carlo simulation of parameter confidence intervals for non-linear regression analysis of biological data using Microsoft Excel. Comput. Methods Programs Biomed. 2012;107:155–63. https://doi.org/10.1016/j.cmpb.2011.05.009
64. Foo KY, Hameed BH. Insights into the modeling of adsorption isotherm systems. Chem. Eng. J. 2010;156:2–10. https://doi.org/10.1016/j.cej.2009.09.013
65. Karnib M, Kabbani A, Holail H, Olama Z. Heavy Metals Removal Using Activated Carbon, Silica and Silica Activated Carbon Composite. Energy Procedia 2014;50:113–20. https://doi.org/10.1016/j.egypro.2014.06.014
66. Hyder AHMG, Begum SA, Egiebor NO. Adsorption isotherm and kinetic studies of hexavalent chromium removal from aqueous solution onto bone char. J. Environ. Chem. Eng. 2015;3:1329–36. https://doi.org/10.1016/j.jece.2014.12.005
67. Divband Hafshejani L, Mortazavi P, Sabz ALiPour S, Brooman Nasab S. Isotherm and Kinetics Study of The Adsorption of Chromium (VI) From Aqueous Solution by Zizyphus Spina-christi Leaves Ash Nanoparticles. Irrig. Sci. Eng. 2016;39:97–110. https://doi.org/10.22055/jise.2016.12499
68. Taha AA, Shreadah MA, Ahmed AM, Heiba HF. Multi-component adsorption of Pb(II), Cd(II), and Ni(II) onto Egyptian Na-activated bentonite; Equilibrium, kinetics, thermodynamics, and application for seawater desalination. J. Environ. Chem. Eng. 2016;4:1166–80. https://doi.org/10.1016/j.jece.2016.01.025
69. Nag S, Mondal A, Bar N, Das SK. Biosorption of chromium (VI) from aqueous solutions and ANN modelling. Environ. Sci. Pollut. Res. 2017;24:18817–35. https://doi.org/10.1007/s11356-017-9325-6
70. Srivastava S, Agrawal SB, Mondal MK. Synthesis, characterization and application of Lagerstroemia speciosa embedded magnetic nanoparticle for Cr(VI) adsorption from aqueous solution. J. Environ. Sci. China 2017;55:283–93. https://doi.org/10.1016/j.jes.2016.08.012
71. Ahsan MdA, Jabbari V, Islam MdT, Kim H, Hernandez-Viezcas JA, Lin Y, et al. Green synthesis of a highly efficient biosorbent for organic, pharmaceutical, and heavy metal pollutants removal: Engineering surface chemistry of polymeric biomass of spent coffee waste. J. Water Process Eng. 2018;25:309–19. https://doi.org/10.1016/j.jwpe.2018.08.005
72. Boeykens SP, Saralegui A, Caracciolo N, Piol MN. Agroindustrial waste for lead and chromium biosorption. J. Sustain. Dev. Energy Water Environ. Syst. 2018;6:341–50. https://doi.org/10.13044/j.sdewes.d5.0184
73. Mahmood-Ul-Hassan M, Suthar V, Ahmad R, Yousra M. Biosorption of metal ions on lignocellulosic materials: batch and continuous-flow process studies. Environ. Monit. Assess. 2018;190. https://doi.org/10.1007/s10661-018-6674-7
74. Mortazavian S, An H, Chun D, Moon J. Activated carbon impregnated by zero-valent iron nanoparticles (AC/nZVI) optimized for simultaneous adsorption and reduction of aqueous hexavalent chromium: Material characterizations and kinetic studies. Chem. Eng. J. 2018;353. https://doi.org/10.1016/j.cej.2018.07.170
75. Sadiq A, Choubey A, Bajpai AK, Sadiq A, Choubey A, Bajpai AK. Biosorption of chromium ions by calcium alginate nanoparticles. J. Chil. Chem. Soc. 2018;63:4077–81. https://doi.org/10.4067/s0717-97072018000304077
76. Abilio TE, Soares BC, José JC, Milani PA, Labuto G, Carrilho ENVM. Hexavalent chromium removal from water: adsorption properties of in natura and magnetic nanomodified sugarcane bagasse. Environ. Sci. Pollut. Res. 2021;28:24816–29. https://doi.org/10.1007/s11356-020-11726-8
77. Dan-Iya BI, Shukor MY. Isothermal Modelling of the Adsorption of Chromium onto Calcium Alginate Nanoparticles. J. Environ. Microbiol. Toxicol. 2021;9:1–7. https://doi.org/10.54987/jemat.v9i2.607
78. Mahmoud ME, El-Said GF, Ibrahim GAA, Elnashar AAS. Effective removal of hexavalent chromium from water by sustainable nano-scaled waste avocado seeds: adsorption isotherm, thermodynamics, kinetics, and error function. Biomass Convers. Biorefinery 2022. https://doi.org/10.1007/s13399-022-03619-2